Supporting Information

Breaking the Scaling Relations via Dual Metal Doping to Cobalt Spinel for OER: a Computational Prediction

Yikun Kang, Feiran Zhang, Bowen Liu, Yuanqing Sun, Xiao Zhang, Weiyu Song[*], Yuechang Wei, Zhen Zhao, Jian Liu[*]

State Key Laboratory of Heavy Oil Processing, China University of Petroleum, Beijing 102249, China

*Corresponding Author: songwy@cup.edu.cn (Weiyu Song); liujian@cup.edu.cn (Jian Liu)

COMPUTATIONAL DEATILS

Surface structure as a function of U_{SHE} and pH

To identify the most stable surface at a certain USHE and pH, we established the phase structure as a function of pH and U as in Rong et al.[1] We consider the surface reconstruction as two processes, namely the surface ion exchange and solvation processes, and the corresponding Gibbs free energy changes are ΔG_1 and ΔG_2, respectively. The total Gibbs free energy change ΔG of the surface reconstruction can be expressed as $\Delta G = \Delta G_1 + \Delta G_2$, where

$$\Delta G_1 = G_{S_I} - G_{S_F} + \mu_A - \mu_B \tag{S1}$$

$$\Delta G_2 = \sum_i (\Delta G_{SHE,i}^\circ + kTln\alpha_{H_xiO_y^{z-}}) - n_{e(e}U_{SHE)} - 2.3^{n}H^+ kTpH \tag{S2}$$

In the expression of ΔG_1, G_{S_I} and G_{S_F} are the free energies of the initial clean Co$_3$O$_4$ (110)-B surface and reconstructed surfaces. μ_A and μ_B is the chemical potential for the exchanged species A and B.

ΔG_2 is computed from experimental thermodynamic data of the species associated with exchanged i (species A and B are collectively referred to as i for conciseness) at standard state relative to the standard hydrogen electrode (SHE), and the expression of the free energy of related solvated ions in ΔG_2 is shown in table Table S1, where ΔG_{SHE}° is obtained from experiments.[2]

Table S1. Summarized ΔG_2 of the related solvated species of Co_3O_4 at T= 25°C.

A	Aqueous species	ΔG°_{SHE}/eV	ΔG_2/eV
Co	Co^{2+}	-0.56	$-2eU_{SHE} + 0.026ln\alpha_{Co2+} - 0.56$
	$Co(OH)_2$	0.15	$-2eU_{SHE} - 0.118pH + 0.15$
	$HCoO_2^-$	0.69	$-2eU_{SHE} - 0.177pH + 0.026ln\alpha_{Co2+} + 0.69$
	Co_3O_4	0.53	$-2.67eU_{SHE} - 0.157pH + 0.53$
	$CoOOH$	0.92	$-3eU_{SHE} - 0.177pH + 0.92$
	Co^{3+}	1.39	$-3eU_{SHE} + 0.026ln\alpha_{Co3+} + 1.39$
	HCo_2O_4	1.83	$-3.5eU_{SHE} - 0.207pH + 1.83$
	CoO_2	2.67	$-4eU_{SHE} - 0.236pH + 2.67$
O	H_2O	0	$2eU_{SHE} + 0.118pH$

Calculation of the free energy change in OER process

The OER process is generally considered to be a four-step electron transfer mechanism. The Gibbs free energy differences of these intermediates including zero point energy (ZPE) and entropy corrections (TΔS) can be calculated as

$$\Delta G_i = \Delta E_i + \Delta ZPE_i - T\Delta S_i \text{ (S3)}$$

In this work, the Gibbs free energy change of OER following AEM can be expressed as[3]

$$\Delta G_1 = \Delta G_{O^*} - \Delta G_{OH^*} - eU + \Delta G_{pH} \text{ (S4)}$$

$$\Delta G_2 = \Delta G_{OOH^*} - \Delta G_{O^*} - eU + \Delta G_{pH} \text{ (S5)}$$

$$\Delta G_3 = 4.92 - \Delta G_{OOH^*} - eU + \Delta G_{pH} \text{ (S6)}$$

$$\Delta G_4 = \Delta G_{OH^*} - eU + \Delta G_{pH} \text{ (S7)}$$

In LOM, we calculate the free energy change of each elementary step as follows[4,5]

$$\Delta G_1 = \Delta G_{O^*} - \Delta G_{OH^*} - eU + \Delta G_{pH} \text{ (S8)}$$

$$\Delta G_2 = \Delta G_{[O-O]^*} - \Delta G_{O^*} + \Delta G_{pH} \text{ (S9)}$$

$$\Delta G_3 = 4.92 + \Delta G_{[V_O-O]^*} - \Delta G_{[O-O]^*} + \Delta G_{pH} \text{ (S10)}$$

$$\Delta G_4 = \Delta G_{[OH+V_O]^*} - \Delta G_{[V_O-O]^*} - eU + \Delta G_{pH} \text{ (S11)}$$

$$\Delta G_5 = \Delta G_{[H+OH]^*} - \Delta G_{[OH+V_O]^*} - eU + \Delta G_{pH} \text{ (S12)}$$

$$\Delta G_6 = \Delta G_{OH^*} - \Delta G_{[H+OH]^*} - eU + \Delta G_{pH} \text{ (S13)}$$

where U is the potential measured against normal hydrogen electrode (NHE) at standard conditions. The free energy change of the protons relative to the NHE at non-zero pH follows Nernst equation as $\Delta G_{pH} = -k_B T \ln(10) \times pH$.

The catalytic performance was estimated by the free energy change of potential-determining step (PDS) in the OER process, and $\Delta G_{PDS} = \max [\Delta G_1, ..., \Delta G_n]$, where n

represent the corresponding electron transfer steps in AEM and LOM. Then the overpotential is expressed as:

$$\eta = \frac{\Delta G_{PDS}}{e} - 1.23 \ [V] \ (S14)$$

As commonly practiced, the standard chemical potential of H_2O (l) is equivalent to the DFT total energy of $H_2O(g)$ together with corrections for the zero-point energy (ZPE) and entropy at 25°C and 0.035 atm, and we use the following ZPE uniformly as shown in Table S2.

Table S2. Corrections for zero-point energy and entropy (T = 298.15 K). Energies are in eV.

	TS	ZPE
H_2O (l)	0.67	0.57
H_2 (g)	0.40	0.28
OH*	0	0.34
O*	0	0.06
OOH*	0	0.42

Calculation of the doping energy:

The doping energy (E_d) is calculated as follows:

$$E_d = E(\text{doped surface}) + \sum_i E(Co\ atom) - E(\text{undoped surface}) - \sum_i E(doped\ atom)$$

where E(doped surface) is the total energy of the doped type, and $\sum_i E(Co\ atom)$ and $\sum_i E(doped\ atom)$ are referred to the energy of the exchanged Co atom(s) and doping atom(s) respectively. The negative value of E_d indicates the exothermic character of the doping, meaning a relatively stable doped structure.

Table S3. Bader charge of the Co4f in the clean (110) surface and the Co5f transformed from Co4f in the most stable surface structure Co_3O_4-2Co+2H, the corresponding Co1 and Co2 atoms are shown in Figure S2.

Bader charge	Co1	Co2
Ideal Co_3O_4 (110)-B	1.303 (~2+)	1.303 (~2+)
Co_3O_4-2Co+2H	1.494 (~3+)	1.415 (~3+)

Table S4. Free energy change of the OER process following **AEM**[a] at different sites on the reconstructed Co_3O_4 surface.

AEM site	ΔG_1 [eV]	ΔG_2 [eV]	ΔG_3 [eV]	ΔG_4 [eV]
Co5f_Top	1.66	1.03	-0.16	**2.39**
Co5f_Bri	1.57	**1.66**	1.11	0.57
Co6f_Bri	**1.82**	1.64	0.33	1.12

[a] All steps and free energy changes correspond to **AEM** in scheme 1. The structural details are shown in Figure S3.

Table S5. Free energy change of the OER process following **LOM**[a] at different sites on the reconstructed Co_3O_4 surface.

LOM site	ΔG_1	ΔG_2	ΔG_3	ΔG_4	ΔG_5	ΔG_6
Co5f	1.57	0.05	0.13	0.48	1.17	**1.63**
Co6f	**1.82**	0.80	0.37	0.04	0.48	1.53

[a] All steps and free energy changes correspond to **LOM** in scheme 1. The structural details are shown in Figure S4.

Table S6. Summary of the free energy change of the OER process on the investigated types following **AEM**[a].

Samples	ΔG_1 [eV]	ΔG_2 [eV]	ΔG_3 [eV]	ΔG_4 [eV]	η_{AEM} [V]
Cr	1.43	**1.99**	0.78	0.72	0.76
Mn	**1.77**	1.58	0.83	0.74	0.54
Fe	**2.08**	1.41	0.75	0.68	0.85
Ni	**1.99**	1.46	0.56	0.91	0.76
Cu	**2.20**	0.99	0.55	1.17	0.97
Zn	**1.77**	1.48	0.26	1.41	0.54
Mo	1.68	**1.89**	1.21	0.14	0.66
Ru	0.90	**2.38**	0.83	0.81	1.15
Rh	1.52	**2.10**	0.84	0.46	0.87
Pd	**1.69**	1.56	0.91	0.76	0.46
Ag	**1.91**	1.61	0.26	1.14	0.68
Cd	**1.84**	1.61	0.15	1.32	0.61
Zn-Cr	1.53	**1.94**	0.18	1.28	0.71
Zn-Mn	**2.04**	1.54	-0.64	1.97	0.81
Zn-Fe	**2.01**	1.58	0.49	0.84	0.78
Zn-Ni	**2.31**	1.06	0.22	1.33	1.08
Zn-Cu	**2.63**	0.79	0.10	1.40	1.40
Zn-Mo	1.77	**1.91**	0.82	0.42	0.68
Zn-Ru	1.28	**2.31**	0.28	1.04	1.08
Zn-Rh	1.64	**1.83**	0.78	0.67	0.60
Zn-Pd	**2.01**	1.34	0.81	0.76	0.78
Zn-Ag	**2.36**	0.99	0.35	1.22	1.13

[a] All steps and free energy changes correspond to **AEM** in scheme 1.

Table S7. Summary of the free energy change of the OER process on the investigated types following **LOM**[a].

Samples	ΔG_1 [eV]	ΔG_2 [eV]	ΔG_3 [eV]	ΔG_4 [eV]	ΔG_5 [eV]	ΔG_6 [eV]	η_{LOM} [V]
Cr	1.43	0.41	0.89	0.05	0.48	**1.65**	0.42
Mn	**1.77**	0.24	0.09	0.47	0.58	1.76	0.54
Fe	**2.08**	0.05	0.03	0.29	0.76	1.71	0.85
Ni	**1.99**	-0.66	0.02	0.63	1.06	1.88	0.76
Cu	**2.20**	-1.25	0.18	0.79	1.29	1.71	0.97
Zn	1.77	-0.75	0.27	0.60	1.23	**1.80**	0.57
Mo	1.68	0.82	0.59	-0.07	0.12	**1.78**	0.55
Ru	0.90	**1.62**	1.30	0.05	0.04	1.01	0.39
Rh	**1.52**	0.87	0.52	0.34	0.42	1.26	0.29
Pd	**1.69**	0.26	0.53	0.26	0.62	1.56	0.46
Ag	**1.91**	-0.50	0.13	0.77	1.29	1.34	0.68
Cd	**1.84**	-0.37	0.39	0.33	1.07	1.66	0.61
Zn-Cr	**1.53**	-0.12	0.55	0.30	1.35	1.31	0.30
Zn-Mn	2.04	-1.10	0.72	0.41	0.66	**2.18**	0.95
Zn-Fe	**2.01**	-0.60	0.59	-0.01	1.22	1.70	0.78
Zn-Ni	2.31	-1.33	-0.48	0.99	1.11	**2.32**	1.09
Zn-Cu	**2.63**	-1.97	-0.36	1.21	1.34	2.07	1.40
Zn-Mo	1.77	0.21	0.54	-0.04	0.41	**2.02**	0.79
Zn-Ru	**1.28**	0.97	1.10	0.31	0.20	1.05	0.05
Zn-Rh	**1.64**	0.26	0.31	0.57	0.51	1.63	0.41
Zn-Pd	2.01	-0.60	0.45	0.45	0.59	**2.03**	0.80
Zn-Ag	**2.36**	-1.54	0.01	1.11	1.59	1.39	1.13

[a] All steps and free energy changes correspond to **LOM** in scheme 1.

Table S8. Summary of the energy barrier of O-O coupling ($\Delta G_{O-O}^{\ddagger}$) and imaginary frequency (IF) of the transition state on the investigated types.

Samples	ΔG_{O*} (eV)	$\Delta G_{O-O}^{\ddagger}$ (eV)	Imaginary Frequency
Cr	2.15	1.62	418.3 cm-1
Mn	2.51	1.37	532.3 cm-1
Fe	2.76	1.14	702.9 cm-1
Co	2.68	1.37	370.8 cm-1
Ni	2.90	0.79	446.5 cm-1
Cu	3.38	0.31	429.1 cm-1
Zn	3.18	0.92	491.1 cm-1
Mo	1.82	1.98	169.9 cm-1
Ru	1.71	2.52	729.9 cm-1
Rh	1.98	2.08	600.9 cm-1
Pd	2.45	1.85	700.4 cm-1
Ag	3.05	0.75	307.1 cm-1
Cd	3.15	0.46	555.8 cm-1
Zn-Cr	2.52	1.33	481.7 cm-1
Zn-Mn	4.01	0.83	534.4 cm-1
Zn-Fe	2.85	0.88	509.6 cm-1
Zn-Ni	3.64	0.61	480.5 cm-1
Zn-Cu	4.03	0.11	578.5 cm-1
Zn-Mo	2.19	1.75	200.4 cm-1
Zn-Ru	2.33	2.10	370.2 cm-1
Zn-Rh	2.31	1.62	648.5 cm-1
Zn-Pd	2.77	1.23	126.1 cm-1
Zn-Ag	3.58	0.87	991.8 cm-1

Table S9. Summarized magnetic moment of each doped metal.

Sample	Magnetic moment (μ_B)	Sample	Magnetic moment (μ_B)
Cr	2.49	Zn-Cr	0.01, 2.51
Mn	3.91	Zn-Mn	0.00, 3.84
Fe	4.24	Zn-Fe	0.01, 3.50
Ni	1.82	Zn-Ni	0.01, 1.73
Cu	0.59	Zn-Cu	0.00, 2.52
Zn	0.01	Zn-Mo	0.01, 2.31
Mo	2.32	Zn-Ru	0.03, 1.55
Ru	0.49	Zn-Rh	0.02, 0.71
Rh	0.25	Zn-Pd	0.00, 0.61
Pd	0.54	Zn-Ag	0.01, 0.02
Ag	0.06	Co	2.80 (undoped active site)
Cd	0.01		
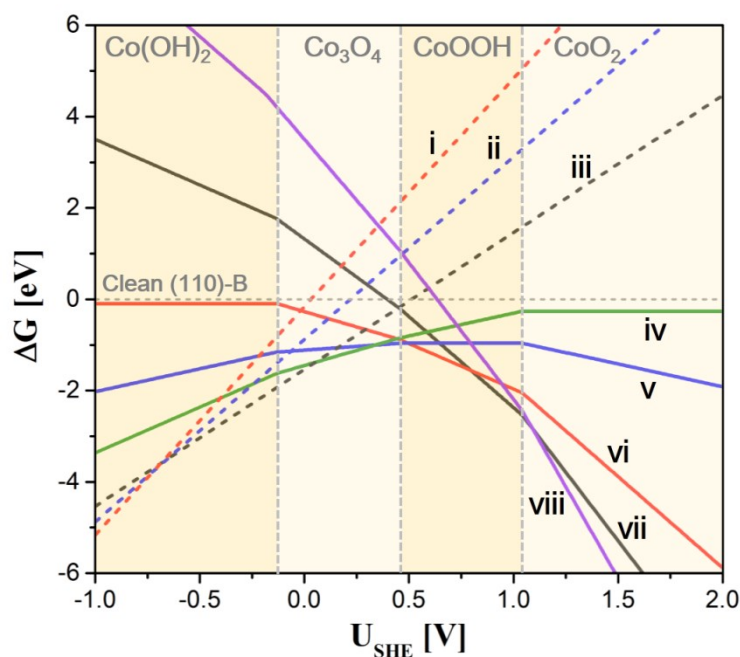
Figure S1. Relationship between free energy change of surface reconstruction and U_{SHE} at pH = 12, with the clean (110)-B surface as reference. (i)-(viii) are the most stable surface structures at different potentials. The colored regions represent different solvated species.

Figure S1 shows the free energy change of the surface reconstruction as a function of U_{SHE} at pH = 12. The slope of each surface structure is determined by the total number of electrons exchanged during the solvation process. Thereby the curved lines in Figure S1 indicates that the exchanged cobalt ions are converted into solvated species with different valences at different potentials.
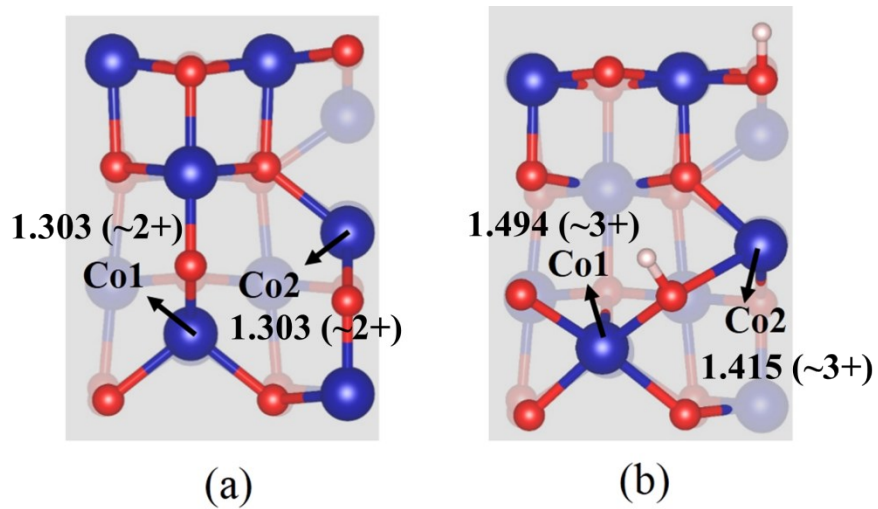
Figure S2. The corresponding converted cobalt atoms in Bader charge (q) analysis on the (a) ideal Co_3O_4 (110) surface and (b) reconstructed surface ($Co_3O_4 - 2Co + 2H$).
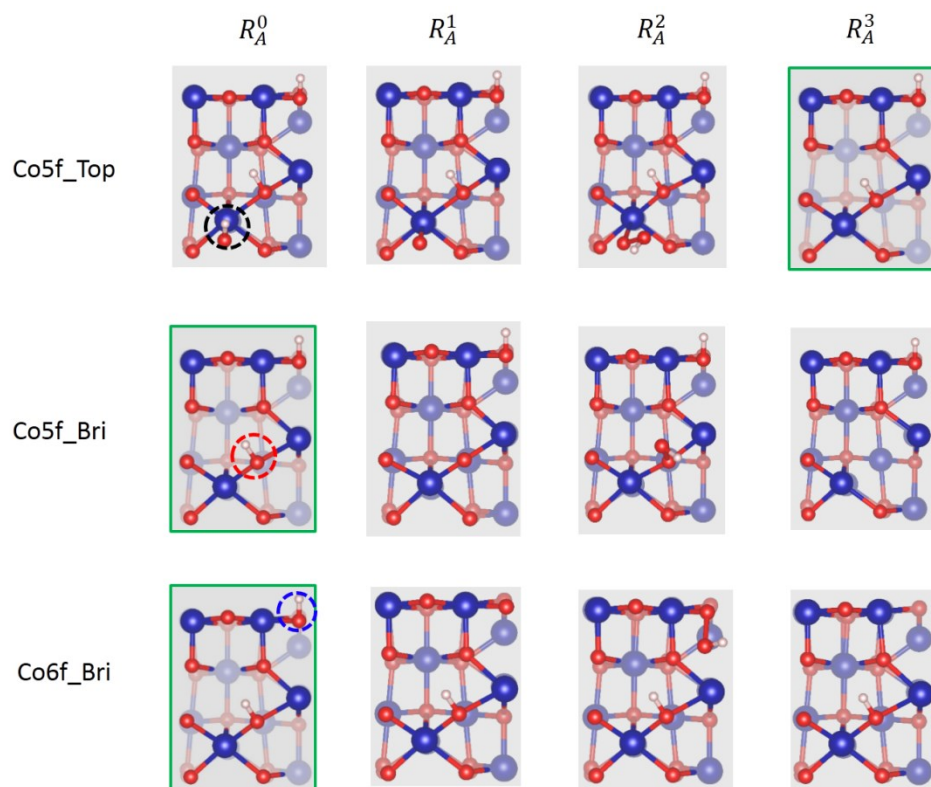
Figure S3. OER process at different sites (Co5f_Top, Co5f_Bri and Co6f_Bri) following AEM on the most stable surface.
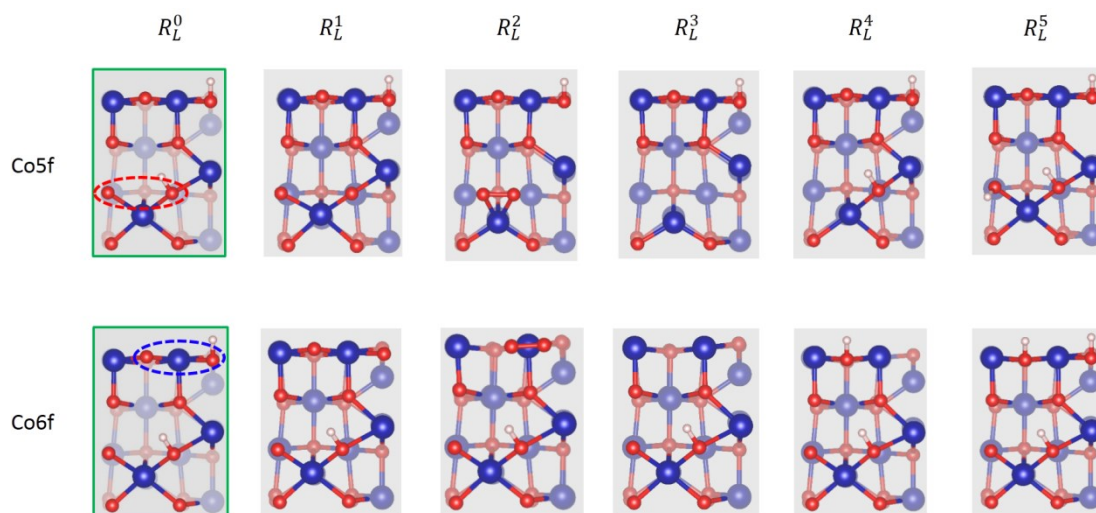
Figure S4. OER process at different sites (Co5f and Co6f) following LOM on the most stable surface.
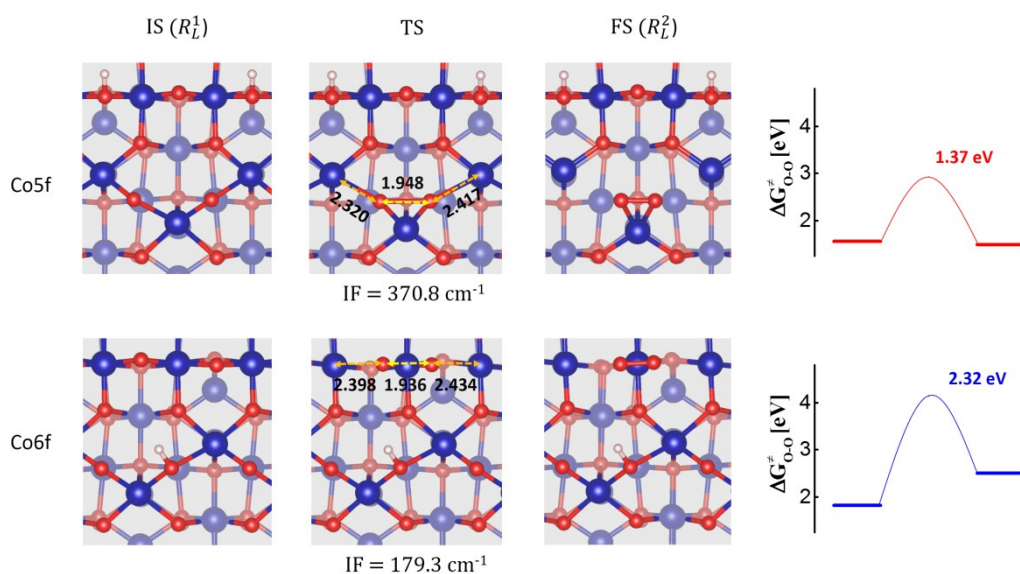
Figure S5. Transition state structures of O-O coupling in LOM at Co5f and Co6f respectively, and corresponding free energy barrier ($\Delta G_{O-O}^{\ddagger}$). IS: initial state; TS: transition state; FS: final state; the unit of bond length is Å.
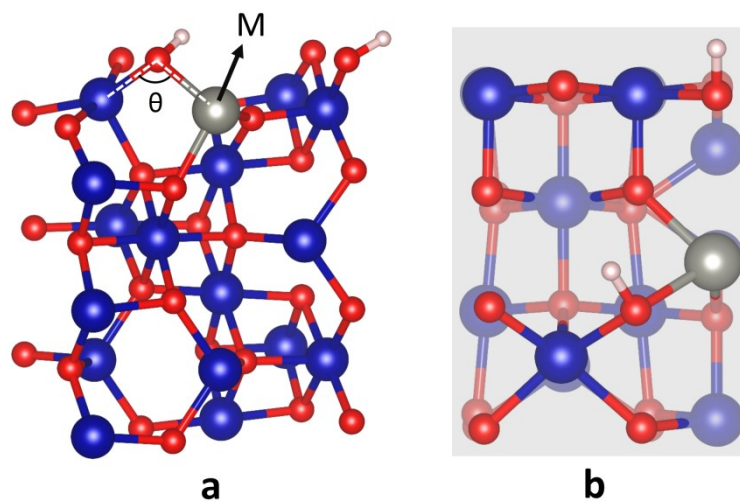
Figure S6. Schematic diagram of single doping type from (a) side view and (b) top view.
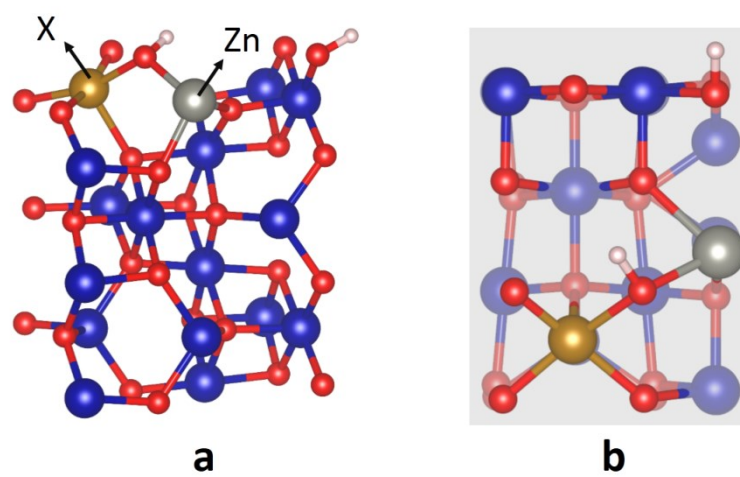
Figure S7. Schematic diagram of double doping type from (a) side view and (b) top view.
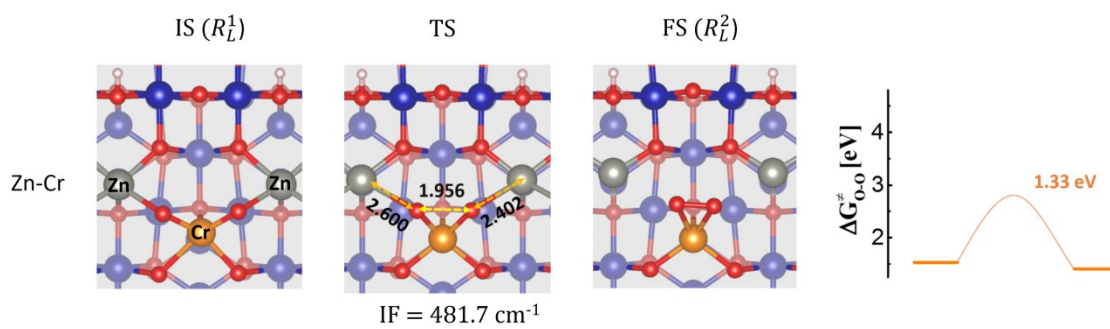
Figure S8. Transition state structures of O-O coupling in LOM of Zn-Cr dual doping type, and corresponding free energy barrier ($\Delta G_{O-O}^{\ddagger}$). IS: initial state; TS: transition state; FS: final state; the unit of bond length is Å.
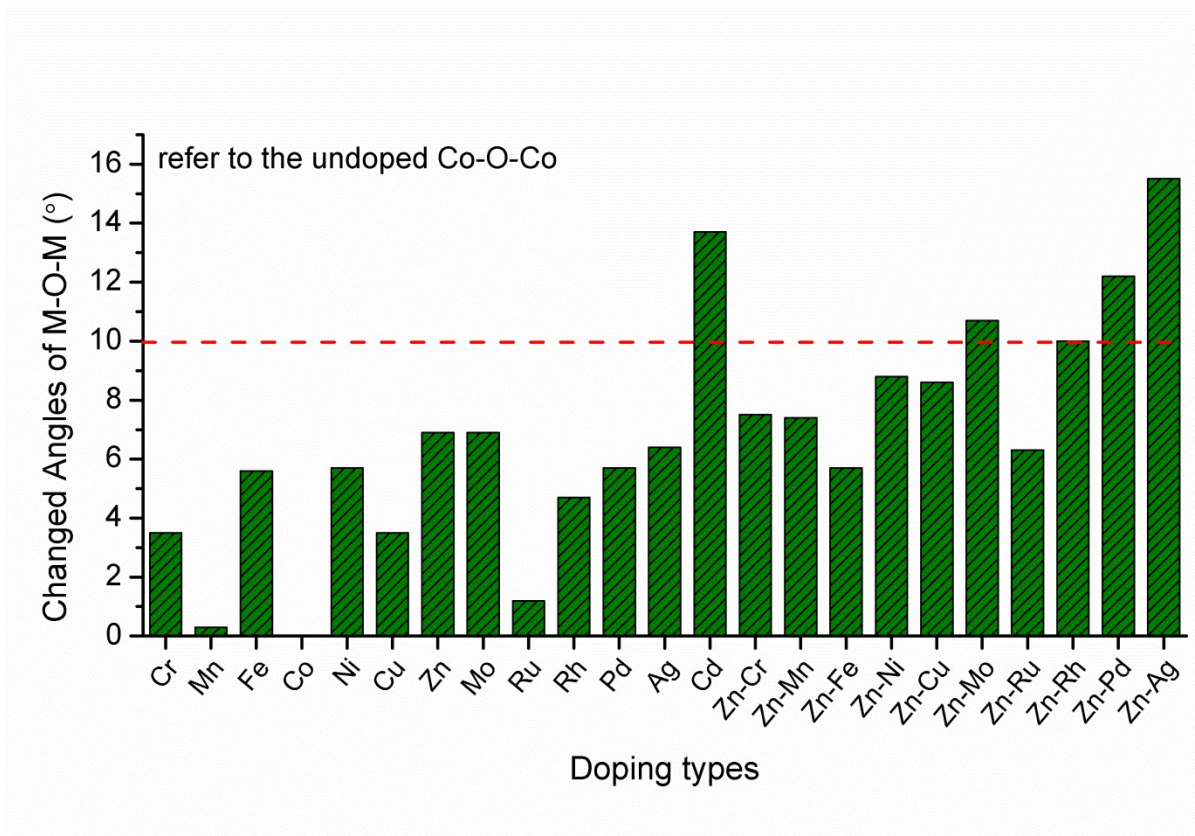
Figure S9. Summary of changes in M-O-M bond angle after doping, where the angle of undoped Co-O-Co is used as a reference.
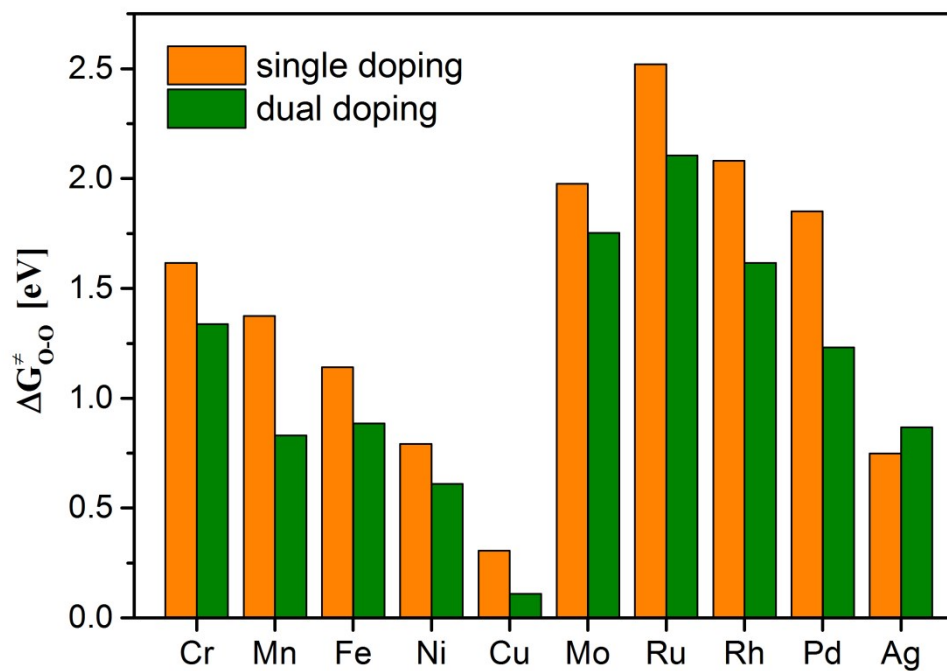
Figure S10. The energy barrier of O-O coupling ($\Delta G_{O\text{-}O}^{\ddagger}$) as a function of the groups for single and dual doping types.
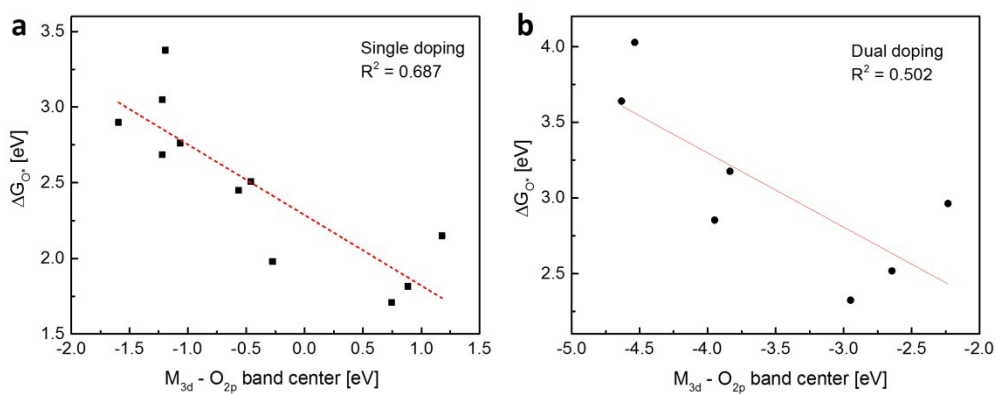
Figure S11. The correlation between the adsorption energy of O* and the difference between the metal d-band center and the oxygen p-band center (M_{3d} - O_{2p}) at the active site in (a) single doped and (b) double doped types.
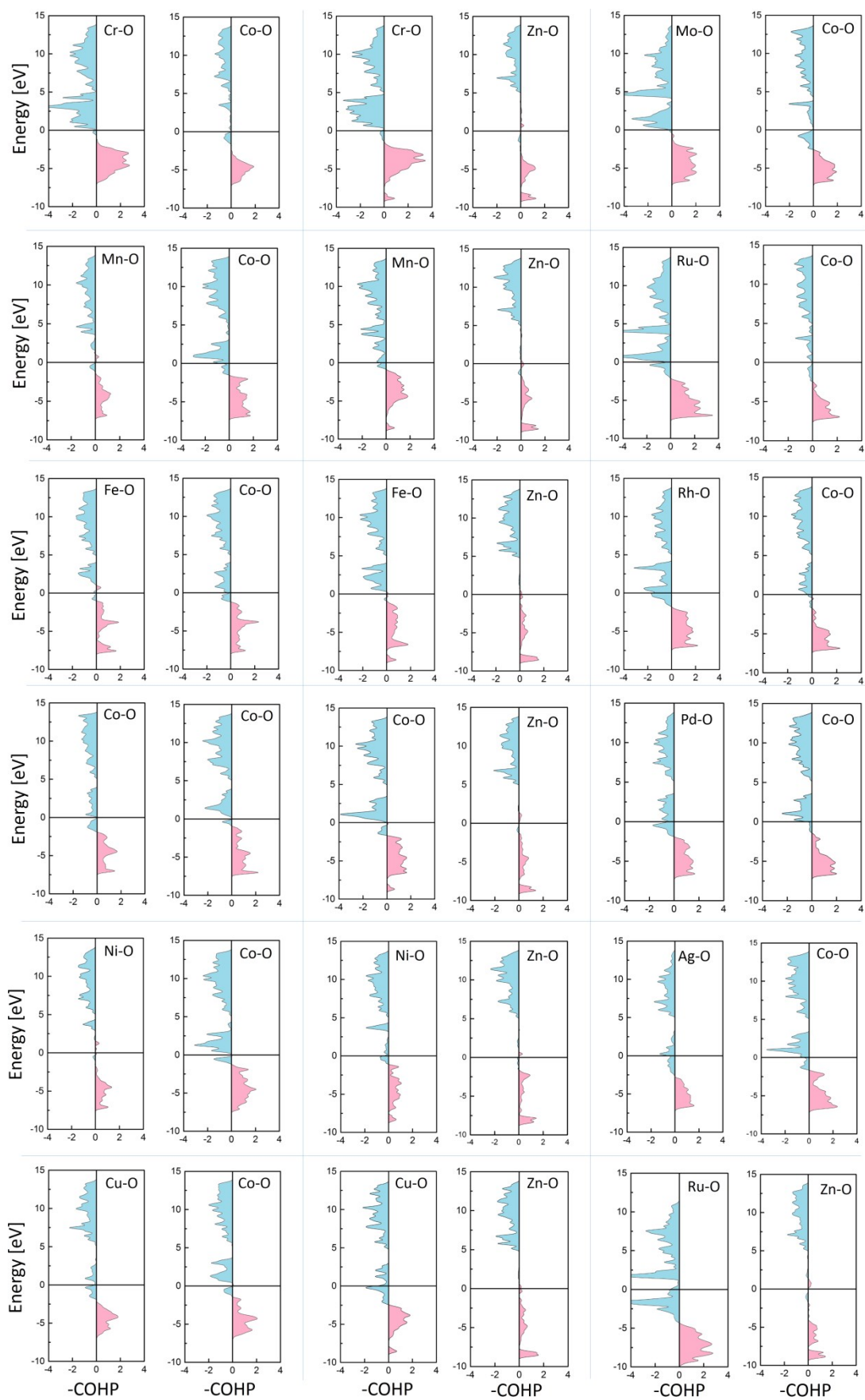
Figure S12. The calculated projected crystal orbital Hamilton population (pCOHP) of the of

the two metal-oxygen bonds at the active site. The positive (negative) represents the bond

(anti-bond) contributions, and the horizontal line represents the Fermi level.
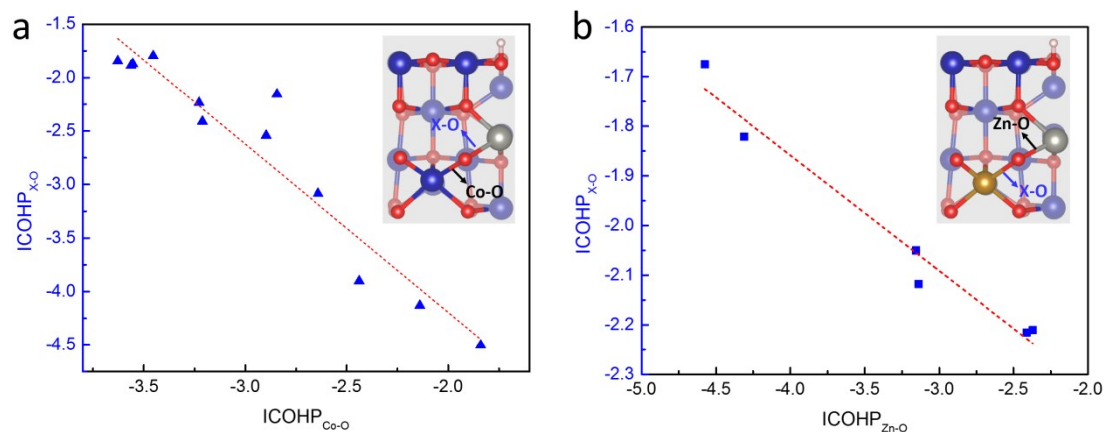
Figure S13. The correlation of the ICOHP of Co-O (ICOHP$_{Co-O}$) and Zn-O (ICOHP$_{Zn-O}$) versus the ICOHP of X-O bond (X is the doped metal) in (a) Co-O-X and (b) Zn-O-X type.

It can be seen that both ICOHP$_{Co-O}$ and ICOHP$_{Zn-O}$ showed a negative correlation with ICOHP$_{X-O}$, which means that the oxygen at the active site is affected by the two metal-oxygen bonds which interact with each other, that is, one is stronger, the other is weaker, so that the investigation of the variation of ΔG_{O*} requires to consider the two bonds comprehensively.
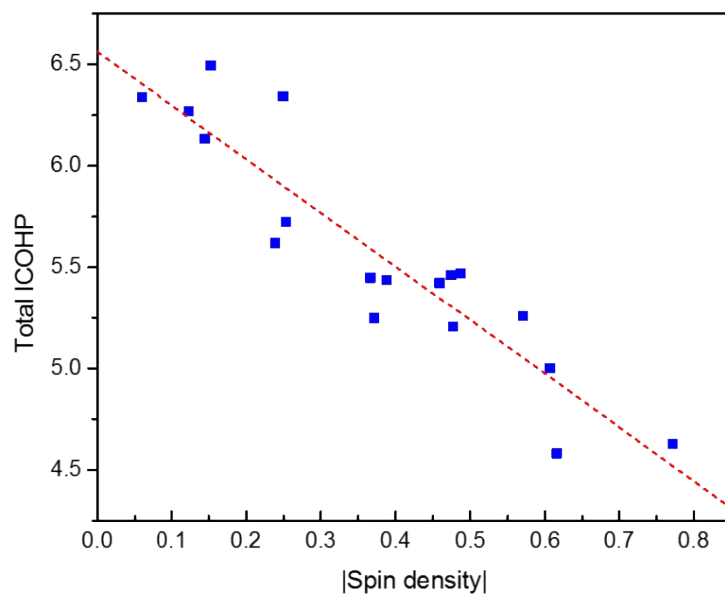
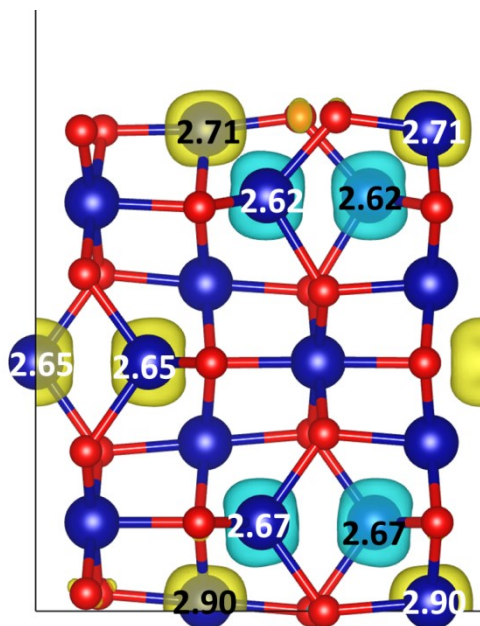**Figure S14.** The correlation between the |Total ICOHP| and |Spin density|.

Figure S15. Side view of spin density of the clean (110)-B of Co_3O_4. Yellow (blue) iso-surfaces denote spin-up (spin-down) of 0.05 e/Bohr^3.
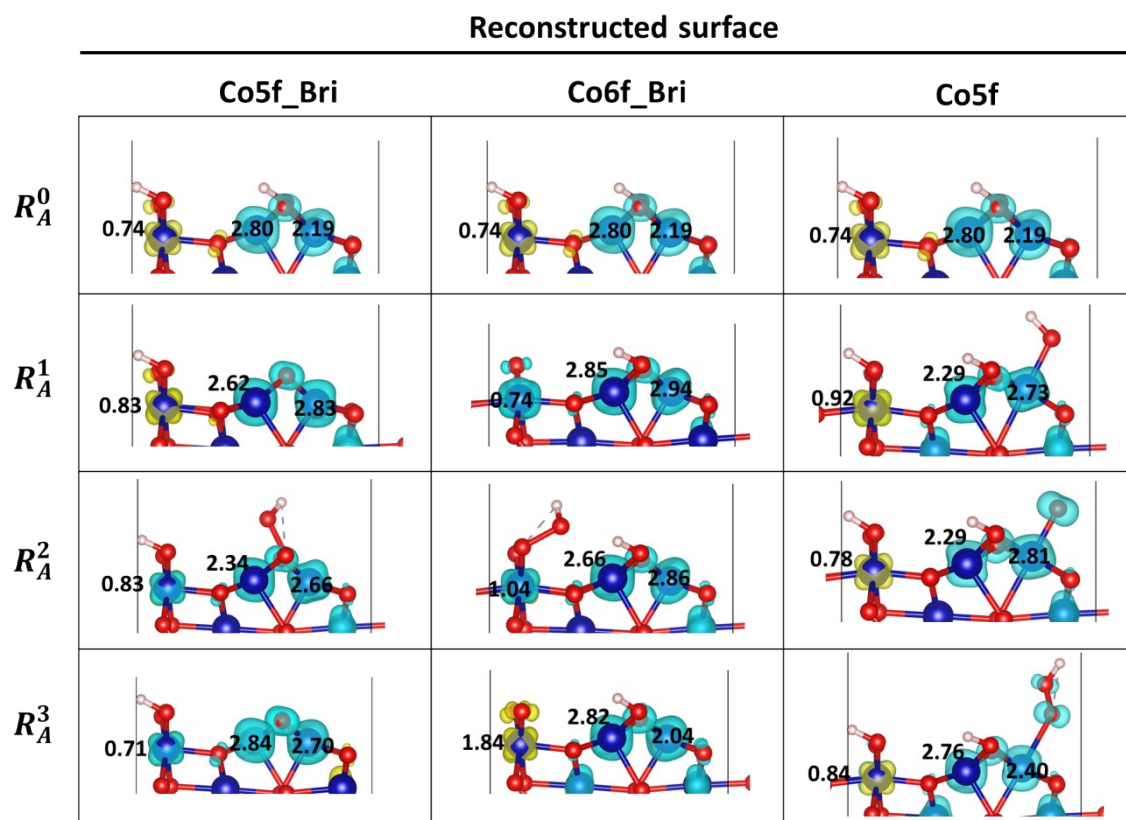
Figure S16. Side view of spin density of reaction intermediates in OER following AEM on the reconstructed surface (Co_3O_4-2Co+2H). Yellow (blue) iso-surfaces denote spin-up (spin-down) of 0.05 e/Bohr^3.

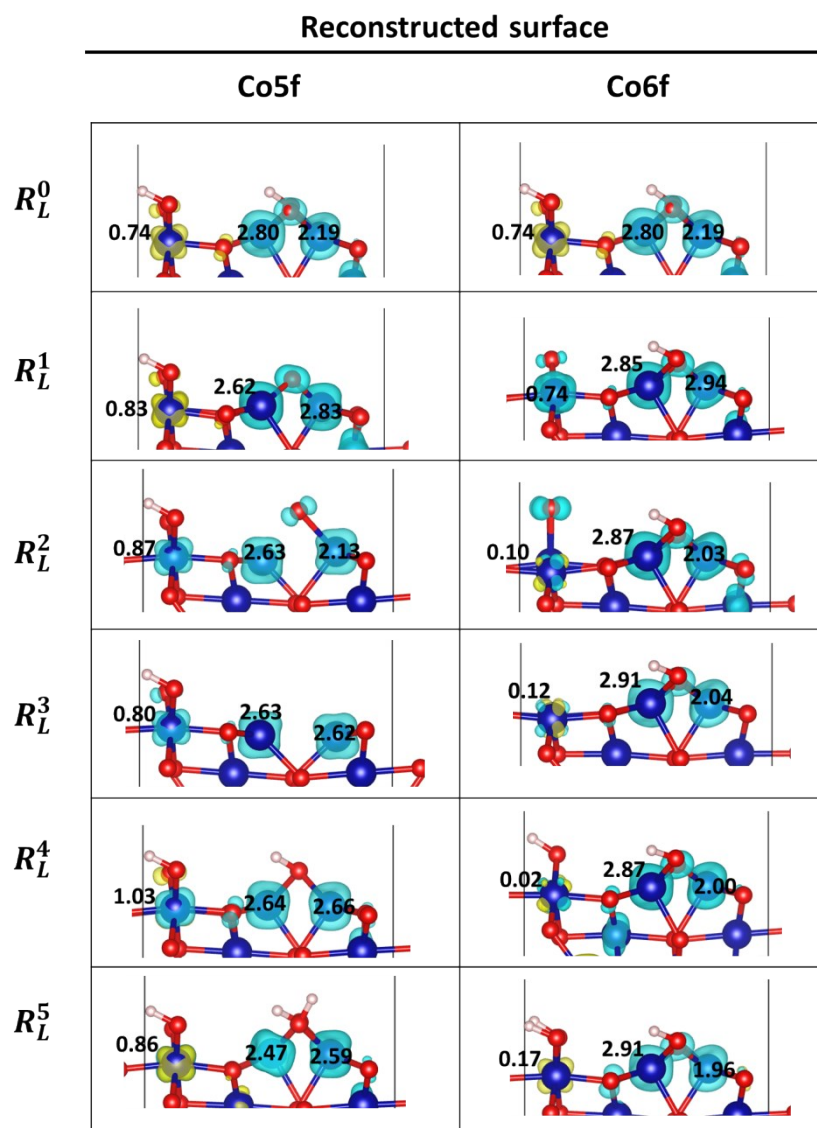**Figure S17.** Side view of spin density of reaction intermediates in OER following LOM on the reconstructed surface (Co_3O_4-2Co+2H). Yellow (blue) iso-surfaces denote spin-up (spin-down) of 0.05 e/Bohr^3.
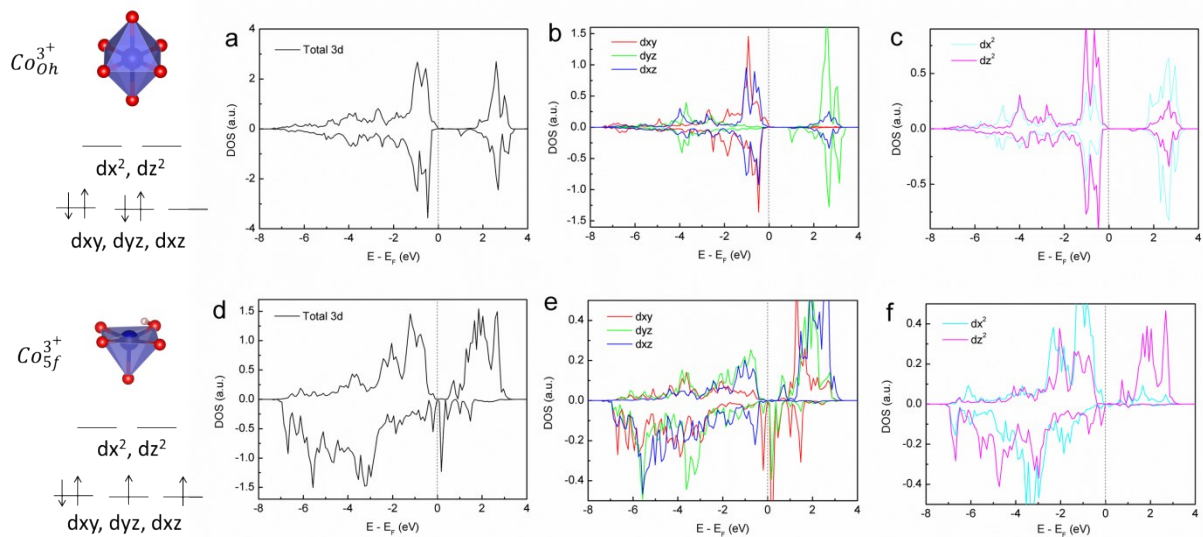
Figure S18. Density state of the Co^{3+} at the octahedral site in the inner layers (Co^{3+}_{Oh}) and the Co^{3+} with five-fold coordinated at the surface layer (Co^{3+}_{5f}).
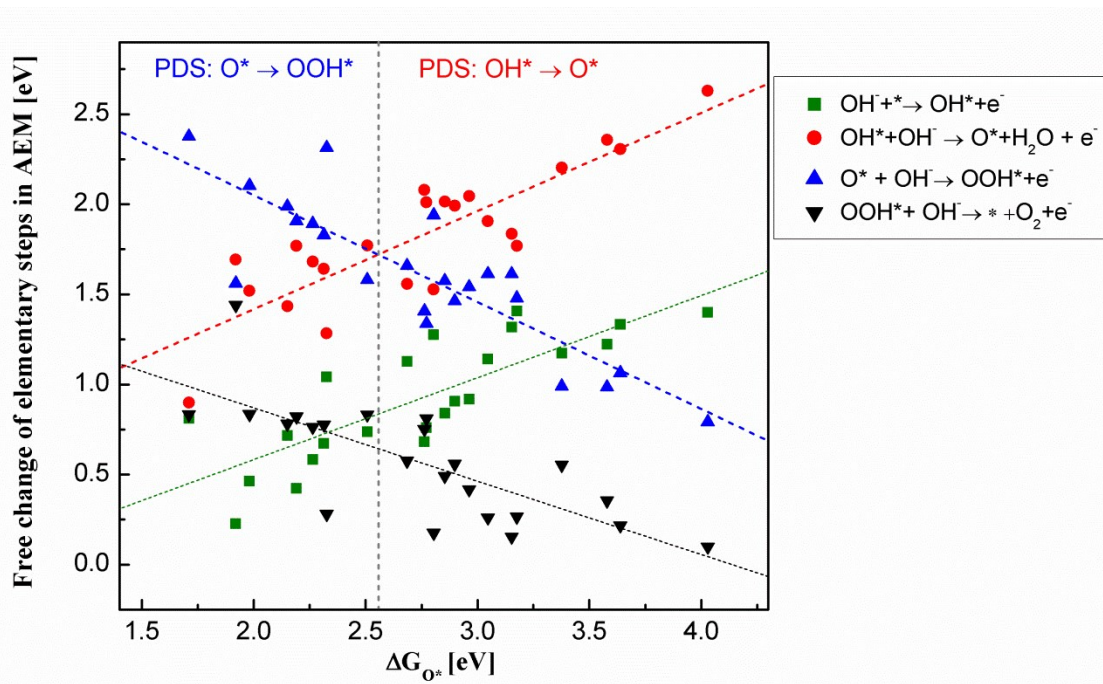
Figure S19. The summarized free energy change of elementary steps in AEM as functions of ΔG_{O*}, where the highest line dictates the PDS.

Coordinates of crucial structures

Ideal Co₃O₄ (110)-B

Co   O
   1.00000000000000
     8.1519002914000005   0.0000000000000000   0.0000000000000000
     0.0000000000000000   5.7642002106000003   0.0000000000000000
     0.0000000000000000   0.0000000000000000   23.9631996154999989
   Co   O
   20   28
Selective dynamics
Direct

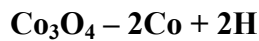|		
0.6250000000000000	0.5000000000000000	0.0066100000000020
0.1250000000000000	0.0000000000000000	0.0066100000000020
-0.0010251309667462	0.5000000000000000	0.1874256241888066
0.7510251309667463	0.0000000000000000	0.1874256241888066
0.1265338714536269	0.0000000000000000	0.3630124136891520
0.6234661285463732	0.5000000000000000	0.3630124136891520
0.8750000000000000	0.2500000000000000	0.0667499970000023
0.8750000000000000	0.7500000000000000	0.0667499970000023
0.1250000000000000	0.0000000000000000	0.1268800049999967
0.6250000000000000	0.5000000000000000	0.1268800049999967
0.3750000000000000	0.2500000000000000	0.1875637939837281
0.3750000000000000	0.7500000000000000	0.1875637939837281
0.6239469255799168	0.5000000000000000	0.2465121966362719
0.1260530744200830	0.0000000000000000	0.2465121966362719
0.8750000000000000	0.7500000000000000	0.3076912793472926
0.8750000000000000	0.2500000000000000	0.3076912793472926
0.5000000000000000	0.0000000000000000	0.0667499970000023
0.2500000000000000	0.5000000000000000	0.0667499970000023
0.4882181935727080	0.0000000000000000	0.3127589327146474
0.2617818064272920	0.5000000000000000	0.3127589327146474
0.3887400030000023	0.5000000000000000	0.0000000000000000
0.3612599969999977	0.0000000000000000	0.0000000000000000
0.8887400030000023	0.0000000000000000	0.0132199999999969
0.8612599969999977	0.5000000000000000	0.0132199999999969
0.1112599969999977	0.7774900200000019	0.0667499970000023
0.6387400030000023	0.7225099799999981	0.0667499970000023
0.6387400030000023	0.2774899899999994	0.0667499970000023
0.1112599969999977	0.2225099950000029	0.0667499970000023
0.8887400030000023	0.0000000000000000	0.1202699990000013
0.8612599969999977	0.5000000000000000	0.1202699990000013
0.3887400030000023	0.5000000000000000	0.1334999950000011
0.3612599969999977	0.0000000000000000	0.1334999950000011
0.6111396574877611	0.7220017650194435	0.1868747490524645

0.6111396574877611	0.2779982049805541	0.1868747490524645
0.1388603425122391	0.7779982349805565	0.1868747490524645
0.1388603425122391	0.2220017800194482	0.1868747490524645
0.3617559543155695	0.0000000000000000	0.2411047078853592
0.3882440456844305	0.5000000000000000	0.2411047078853592
0.8918698405450942	0.0000000000000000	0.2538349986250104
0.8581301594549058	0.5000000000000000	0.2538349986250104
0.1126338495302979	0.7628072680656174	0.3039760167923858
0.1126338495302979	0.2371927469343874	0.3039760167923858
0.6373661504697022	0.7371927319343826	0.3039760167923858
0.6373661504697022	0.2628072380656148	0.3039760167923858
0.8985506940352039	0.0000000000000000	0.3616249700265185
0.8514493059647961	0.5000000000000000	0.3616249700265185
0.4147353176454950	0.5000000000000000	0.3719561611338055
0.3352646823545050	0.0000000000000000	0.3719561611338055

Reconstructed surface under reaction conditions (structure vii in Figure 1):
$Co_3O_4 - 2Co + 2H$

Co   O   H
   1.00000000000000

8.1519002914000005	0.0000000000000000	0.0000000000000000
0.0000000000000000	5.7642002106000003	0.0000000000000000
0.0000000000000000	0.0000000000000000	23.9631996154999989

   Co   O   H
   18   28   2

Selective dynamics
Direct

0.6250000000000000	0.5000000000000000	0.0066100000000020
0.1250000000000000	0.0000000000000000	0.0066100000000020
0.0035853657661220	0.5008609526650520	0.1862910132139625
0.7475374147835631	0.0009075995561599	0.1871291235760524
0.8750000000000000	0.2500000000000000	0.0667499970000023
0.8750000000000000	0.7500000000000000	0.0667499970000023
0.1250000000000000	0.0000000000000000	0.1268800049999967
0.6250000000000000	0.5000000000000000	0.1268800049999967
0.3748612053959388	0.2505907659300156	0.1878565229741285
0.3755108923462699	0.7518796680313982	0.1879540384847173
0.6235134096458960	0.4997057762558909	0.2470541990468065
0.1268786547732342	0.0029407665232709	0.2479083027763877
0.8721420838623742	0.7420392934197071	0.3054778336836659
0.8748752003350097	0.2572941456332485	0.3057970223806464
0.5000000000000000	0.0000000000000000	0.0667499970000023
0.2500000000000000	0.5000000000000000	0.0667499970000023
0.4931384525004747	0.0032784781399176	0.3168946629508292

0.2590429860891975	0.5178821350384791	0.3134628443333329
0.3887400030000023	0.5000000000000000	0.0000000000000000
0.3612599969999977	0.0000000000000000	0.0000000000000000
0.8887400030000023	0.0000000000000000	0.0132199999999969
0.8612599969999977	0.5000000000000000	0.0132199999999969
0.1112599969999977	0.7774900200000019	0.0667499970000023
0.6387400030000023	0.7225099799999981	0.0667499970000023
0.6387400030000023	0.2774899899999994	0.0667499970000023
0.1112599969999977	0.2225099950000029	0.0667499970000023
0.8887400030000023	0.0000000000000000	0.1202699990000013
0.8612599969999977	0.5000000000000000	0.1202699990000013
0.3887400030000023	0.5000000000000000	0.1334999950000011
0.3612599969999977	0.0000000000000000	0.1334999950000011
0.6100221410098904	0.7216156205890010	0.1866077285021765
0.6093151777935455	0.2785128257030176	0.1864520997818209
0.1400046694411148	0.7808322744701317	0.1868524152032432
0.1396084486386956	0.2204601814342980	0.1865415554493187
0.3632061911352141	0.0035172289895090	0.2418465814811379
0.3870725363752313	0.5011299622358102	0.2412640788071931
0.8937824966860726	0.0002285460642066	0.2519763684046761
0.8565365446489357	0.4992445944351352	0.2511053218260785
0.1046616650820780	0.7553234197192110	0.2965145496397903
0.1064657714817770	0.2487089798582201	0.2955223640264132
0.6535336317439835	0.7467104819544494	0.2981826466302371
0.6506868063068182	0.2467692344248099	0.2990925243872691
0.8736401741588516	-0.0000465231004673	0.3579139329460728
0.8909749834762698	0.4973924377350556	0.3524275048897384
0.3774350001047960	0.2924638494020012	0.3548928833573731
0.3807507855275759	-0.2186559747613346	0.3480120740870902
0.4648664458328516	0.3740346865914687	0.3749540418923665
-0.0187824111013202	-0.0000228548813954	0.3762333189967543

REFERENCES

(1) Rong, X.; Kolpak, A. M. Ab Initio Approach for Prediction of Oxide Surface Structure, Stoichiometry, and Electrocatalytic Activity in Aqueous Solution. *J. Phys. Chem. Lett*. **2015**, *6*, 1785-1789.

(2) Wagman, D. D. E., W.H.; Halow, I.; Parker, V.B.; Bailey, S.M.; Schumm, R.H. *Selected Values of Chemical Thermodynamic Properties*; National Bureau of Standards: Washington, U.S.A.; 1968-1971.

(3) Man, I. C.; Su, H.-Y.; Calle-Vallejo, F.; Hansen, H. A.; Martínez, J. I.; Inoglu, N. G.; Kitchin, J.; Jaramillo, T. F.; Nørskov, J. K.; Rossmeisl, J.; Universality in Oxygen Evolution Electrocatalysis on Oxide Surfaces. *ChemCatChem* **2011**, *3*, 1159-1165

(4) Rong, X.; Parolin, J.; Kolpak, A. M. A fundamental relationship between reaction mechanism and stability in metal oxide catalysts for oxygen evolution. *ACS Catal*. **2016**, *6*, 1153-1158.

(5) Huang, Z.-F.; Song, J.; Du, Y.; Xi, S.; Dou, S.; Nsanzimana, J.M. V.; Wang, C.; Xu, Z. J.; Wang, X. Chemical and structural origin of lattice oxygen oxidation in Co–Zn oxyhydroxide oxygen evolution electrocatalysts. *Nature Energy*, **2019**, *4*, 329-338